AIP | Applied Physics Letters

High order sideband generation in terahertz quantum cascade lasers

P. Cavalié, J. Freeman, K. Maussang, E. Strupiechonski, G. Xu et al.

Citation: Appl. Phys. Lett. **102**, 221101 (2013); doi: 10.1063/1.4808385
View online: http://dx.doi.org/10.1063/1.4808385
View Table of Contents: http://apl.aip.org/resource/1/APPLAB/v102/i22
Published by the American Institute of Physics.

Additional information on Appl. Phys. Lett.

Journal Homepage: http://apl.aip.org/
Journal Information: http://apl.aip.org/about/about_the_journal
Top downloads: http://apl.aip.org/features/most_downloaded
Information for Authors: http://apl.aip.org/authors

ADVERTISEMENT

Downloaded 04 Jun 2013 to 129.175.97.14. This article is copyrighted as indicated in the abstract. Reuse of AIP content is subject to the terms at: http://apl.aip.org/about/rights_and_permissions

High order sideband generation in terahertz quantum cascade lasers

P. Cavalié,[1] J. Freeman,[1] K. Maussang,[1] E. Strupiechonski,[2] G. Xu,[2] R. Colombelli,[2] L. Li,[3] A. G. Davies,[3] E. H. Linfield,[3] J. Tignon,[1] and S. S. Dhillon[1]
[1]*Laboratoire Pierre Aigrain, Ecole Normale Supérieure, UMR8551 CNRS, UPMC Univ. Paris 6, Univ. Paris 7, 75231 Paris Cedex 05, France*
[2]*Institut d'Electronique Fondamentale, Univ. Paris Sud, UMR8622 CNRS, 91405 Orsay, France*
[3]*School of Electronic and Electrical Engineering, University of Leeds, Leeds LS9 2JT, United Kingdom*

(Received 20 March 2013; accepted 17 May 2013; published online 3 June 2013)

We demonstrate the generation of high order terahertz (THz) frequency sidebands (up to 3rd order) on a near infrared (NIR) optical carrier within a THz quantum cascade laser (QCL). The NIR carrier is resonant with the interband transition of the quantum wells composing the QCL, allowing the nonlinearity to be enhanced and leading to frequency mixing. A phonon depopulation based QCL with a double metal cavity was used to enhance the intracavity power density and to demonstrate the higher order sidebands. The 1st order sideband intensity shows a linear dependence with THz power corresponding to a single THz photon, while the second order sideband has a quadratic dependence implying a two THz photon interaction and hence a third order susceptibility. These measurements are compared to the photoluminescence and the QCL bandstructure to identify the states involved, with the lowest conduction band states contributing the most to the sideband intensity. We also show that the interaction for the second order sideband corresponds to an enhanced direct third order susceptibility $\chi^{(3)}$ of $\sim 7 \times 10^{-16}(\mathrm{m/V})^2$, two orders of magnitude greater than the bulk value. © *2013 AIP Publishing LLC*. [http://dx.doi.org/10.1063/1.4808385]

Quantum Cascade Lasers (QCLs) are powerful intersubband laser sources operating throughout the mid-infrared (MIR)[1] and terahertz (THz)[2] spectral regions. As well as offering high output powers, they also possess giant optical nonlinearities that are orders of magnitude greater than those of the bulk.[3,4] These arise when the excitation is resonant, i.e., when the incident photon has exactly the same energy as a specific material transition. A wide range of efficient resonant nonlinear effects have been shown, such as second harmonic generation, sum frequency,[5] and difference frequency generation.[6–8] These effects are all based on intersubband nonlinearities and take place within the QCL cavity, taking advantage of the large intracavity power density ($\sim$MW/cm^2).

Recently, the enhanced resonant interband nonlinearities of a THz QCL were used to perform intracavity nonlinear frequency mixing.[9] It was shown that a nonlinear interaction between the THz beam of the QCL, E_{QCL}, and a resonant near-infrared (NIR) excitation, E_{NIR}, of the effective bandgap can occur. This results in the generation of first order THz optical sidebands at energies $E_{NIR} \pm E_{QCL}$. In this case, a QCL based on a bound-to-continuum design was used where the injected NIR was resonant with the miniband and the difference frequency was generated by a virtual state.

High order sideband generation, $E_{NIR} \pm nE_{QCL}$ with integer $n > 1$, is often reported in experiments involving a THz beam provided by a free electron laser (FEL) and using a weak near-infrared laser (see, for example, Refs. 10 and 11). These higher order sidebands can only be generated through the use of the intense THz field interaction with excitons of a quantum well system. Indeed, 18th order sidebands have been recently observed using electron-hole re-collisions where the THz beam was used to accelerate the electron strongly from the bound electron-hole pair.[12] However, the generation of such higher order sidebands, $E_{NIR} \pm nE_{QCL}$ ($n > 1$), has not been observed in any QCL based experiments[13,14] or in FEL measurements involving only electronic states, i.e., when the excitons are screened.[15]

In this letter, we demonstrate the generation of higher order sidebands up to the 3rd order, i.e., $E_{NIR} \pm 3E_{QCL}$. Compared to our previous demonstrations[9] with a bound-to-continuum QCL in a single plasmon waveguide, here a longitudinal-optical (LO) depopulation based QCL with a double metal waveguide is used. As well as allowing high powers,[16] the THz field is confined into a smaller subwavelength volume and results in facet reflectivities approximately three times higher. This leads to intracavity power densities of tens of kW/cm^2. This permits the development of fields within the cavity that are sufficiently large to observe higher order effects. We also deduce the interband resonances involved and show that the nonlinear sidebands are a purely electronic phenomenon.

The GaAs/AlGaAs QCL used is based on a LO-phonon depopulation design operating at 2.9 THz ($E_{QCL} = 12$ meV).[17] The sample was processed into 100 μm wide and 12 μm thick double metal waveguides, and the laser bars were cleaved to a cavity length of 1.5 mm. The samples were cooled to 10 K in a continuous flow helium cryostat. The NIR excitation was provided by a continuous wave Ti:sapphire laser ($\sim$200 μW). The NIR beam is coupled in to the QCL cavity via a high numerical aperture objective (optical density of $\sim$250 W/cm^2) and is coupled out by a reflective objective at the opposite facet. The QCL was operated in pulsed mode with the Ti:sapphire laser synchronized to the QCL's modulation using an acousto-optic modulator. The transmitted difference frequency was then detected by a CCD camera after it has been focused through a NIR spectrometer. A dispersive grating (1800 lines/mm) was used to measure an energy range of 7 meV. The pump and each sideband order are detected

 © 2013 AIP Publishing LLC

Downloaded 04 Jun 2013 to 129.175.97.14. This article is copyrighted as indicated in the abstract. Reuse of AIP content is subject to the terms at: http://apl.aip.org/about/rights_and_permissions

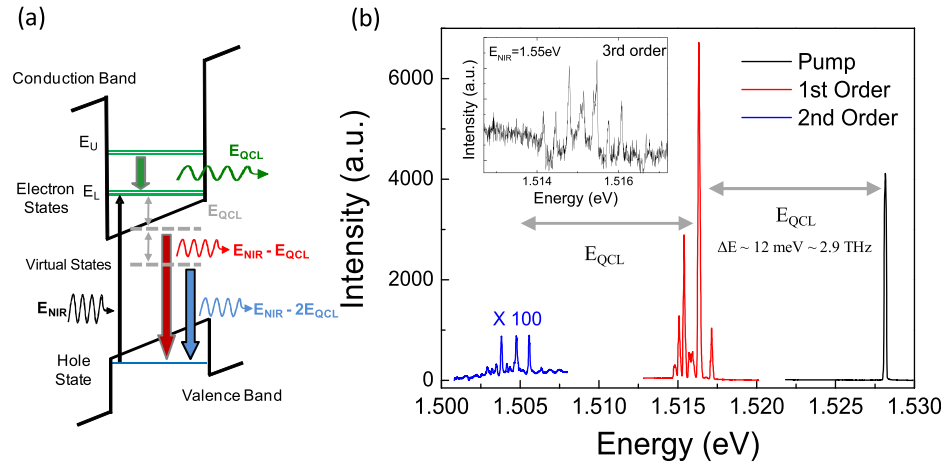

FIG. 1. (a) Schematic of the resonant non-linear process for the generation of the 1st order (E_{NIR}–E_{QCL}) and 2nd order (E_{NIR}–E_{QCL}) sidebands in a QCL operating at E_{QCL} (green arrow between states E_U and E_L). A NIR pump E_{NIR} (black arrow) is in resonance with the interband transitions of the QCL. This allows the generation of a lower energy beams separated from the pump by E_{QCL} and $2E_{QCL}$ (red and blue arrows). b) Sideband spectra with a pump excitation at 811.5 nm (1.528 eV), above the effective band gap of the QCL. The QCL is driven at a current density of 255 A/cm^2 with a 50% duty cycle at a 50 kHz repetition rate. The 1st and 2nd order (intensity ×100) sidebands are separated from the pump by E_{QCL} and $2E_{QCL}$, respectively. Inset: 3rd order harmonic for a pump excitation of 1.55 eV

separately by varying the centre position of the grating in order to allow averaging of the spectra for each order without saturating the CCD with the NIR pump beam.

Figure 1(a) shows the schematic process involved in the nonlinear optical interaction for the first and second order sidebands. An interband excitation in the NIR (black arrow) is resonant with the interband transition between the valence and conduction band of the QCL. The green states indicate the laser transition in the conduction band generating the THz QCL photons. The nonlinear interaction between the NIR and THz photons and the quantum wells within the QCL cavity results in difference frequency generation. The dark red and blue arrows correspond to generation of the first (E_{NIR}–E_{QCL}) and second order sidebands (E_{NIR}–$2E_{QCL}$), respectively, from virtual states (dashed lines) below the gap. The latter point permits the strong interband absorption of the sideband emission to be avoided.

Figure 1(b) shows the typical spectra of the first ($E^{1st} = 1516.3$ meV) and second ($E^{2nd} = 1504.8$ meV) order sidebands, as well as the pump laser beam. The pump is transverse magnetic (TM) polarized for excitation of transitions from light holes.[9] (The pump detected on the CCD camera is a parasitic part of the NIR beam which is not coupled into the QCL waveguide.) Here, the pump energy is slightly larger than the effective bandgap ($E_{NIR} = 1528.2$ meV) such that the first order interaction is maximized.[9] The first and second order sidebands are exactly separated from the pump by E_{QCL} and $2E_{QCL}$, respectively, and only appear when the QCL is operated above laser threshold. The second order sideband is considerably less intense than the first order sideband and required a longer integration time (90 s instead of 1.5 s) to obtain a good signal-to-noise ratio. The first order sideband is a replica of the THz spectrum of the QCL, whilst the second order is more complex with additional modes due to the inter-mixing of the THz QCL Fabry-Pérot modes.[18] The measured efficiencies for each sideband are $P_{1st}/P_{NIR} = 2.6 \times 10^{-4}$ and $P_{2nd}/P_{NIR} = 3.6 \times 10^{-7}$, where P_{NIR} is the transmitted intensity at transparency (i.e., with the energy of the pump below the interband excitation). The third order (E_{NIR}–$3E_{QCL}$) is also observed (see inset of Figure 1(b)) but, owing to its weak intensity, only when the pump energy is well above the bandgap and when the generated beam is close to the bandgap of the material (see below).

Each sideband order exhibits a particular dependence on THz power. Figure 2 shows the sideband intensity as a function of the current density above the laser threshold, where the THz output power of the QCL exhibits a linear behavior. (The inset of Figure 2 shows the THz QCL light-current-voltage (LIV) characteristics with the laser threshold at 215 mA ($J_{th} = 143$ A/cm^2).) The intensity of the 1st order sideband is linear with the current density as expected for a second order nonlinear process, which can be described as $P^{1st} \propto |\chi^{(2)}|^2 P_{QCL} P_{NIR}$ with $\chi^{(2)}$ the second order susceptibility, and P_{QCL} and P_{NIR} are the intensities of the THz and

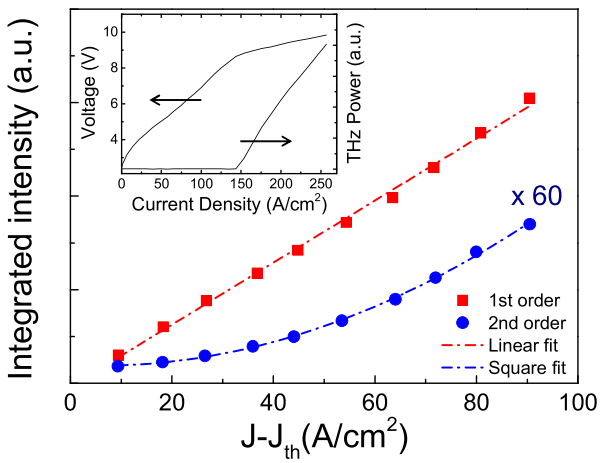

FIG. 2. Integrated spectrum for both orders as a function of current density above laser threshold. The pump excitation energy is such that both sidebands are generated at the same energy (1.516 eV). The second order intensity is multiplied by a factor of 60. Dotted lines are linear and quadratic fits to the 1st and 2nd order data, respectively. The threshold current density (~130 A/cm^2) has been subtracted for clarity and for the fitting. The QCL was operated with a 25% duty cycle at 50 kHz. Inset: L-I-V measurement of the QCL showing a linear dependence of the THz output power as a function of current above threshold.

Downloaded 04 Jun 2013 to 129.175.97.14. This article is copyrighted as indicated in the abstract. Reuse of AIP content is subject to the terms at: http://apl.aip.org/about/rights_and_permissions

NIR pump beams, respectively. The 2nd order sideband instead has a quadratic dependence, in agreement with a third order process involving two THz photons, i.e., $P^{2nd} \propto |\chi^{(3)}|^2 P_{QCL}{}^2 P_{NIR}$, where $\chi^{(3)}$ is the third order susceptibility.

Care was also taken to verify that there was no second harmonic generation of the QCL emission itself, i.e., $2E_{QCL}$ (~24 meV), which was then being upconverted directly to the NIR. The spectra of the QCL were acquired with a Fourier transform infrared (FTIR) spectrometer that showed no emission at twice the QCL frequency. Combined with the intensity behavior explained above, this confirms the third order effect.

An estimation of $\chi^{(3)}$ can be achieved following the formalism of Sutherland *et al.*,[19] where the efficiency is given by

$$\eta_{2nd} = \frac{P_{2nd}}{P_{NIR}} = \frac{16\pi^2 |\chi^{(3)}|^2 L^2 P_{QCL}^2}{\varepsilon_0^2 n_{NIR} n_{QCL}^2 n_{2nd} c^2 \lambda_{2nd}{}^2 S^2} e^{-\alpha_p \frac{L}{2}} \times \frac{\sin^2\left(\frac{\Delta k L}{2}\right) + \sinh^2\left[\alpha_p \frac{L}{4}\right]}{\left(\frac{\Delta k L}{2}\right)^2 + \left(\alpha_p \frac{L}{4}\right)^2}, \quad (1)$$

where P_{2nd} (n_{2nd}), P_{NIR} (n_{NIR}), and P_{QCL} (n_{QCL}) are the intensities (refractive indices) of the second order beam, the input NIR pump, and the THz QCL, respectively, L is the QCL cavity length, λ_{2nd} is the generated wavelength, c is the speed of light, S is the interaction area, Δk is the phase mismatch, and α_p is the NIR pump loss. A similar expression can be obtained for the 1st order efficiency based on the second order nonlinearity $\chi^{(2)}$.[19] Assuming that the pump beam losses (~1000 cm^{-1}) are the predominant factor for the efficiency such that the phase mismatch can be neglected, we infer values of $\chi^{(3)} \approx 8 \times 10^{-16}$ $(m/V)^2$ and $\chi^{(2)} \approx 3 \times 10^{-9}$ m/V, which are both approximately two orders of magnitude greater than the corresponding non-resonant nonlinearities of GaAs. From Eq. (1), we observe that the third order efficiency is proportional to $1/S^2$ while for the second order process the efficiency is proportional to 1/S.[9] This difference in the efficiency explains why the 2nd order sideband is not as efficient in the single plasmon waveguide. Indeed, S^2 is $\sim 8.1 \times 10^7$ μm^2 for a single plasmon waveguide and $S^2 \sim 0.14 \times 10^7$ μm^2 for a double metal waveguide.

The intensities of the 1st and 2nd harmonic were also studied as a function of the pump energy to determine the resonant nature of this optical mixing (Figure 3). The 1st order sideband shows only one resonance (for $E_{NIR} = 1.528$ eV) in intensity while two resonances are observed for the 2nd order sideband (at 1.528 eV and 1.540 eV). The range of pump energies where the second harmonic is observed is considerably wider than for the first order. This is due to the fact that while at high pump energies the 1st harmonic generation is above the effective gap and so completely absorbed by the active region, the 2nd harmonic is still emitted below the gap in the transparency region. Indeed it can be observed that the 1st order sideband intensity drops considerably after its resonance due to its efficiency being convoluted with the absorption from the bandgap edge.

Although difficult to distinguish, the second order sideband appears to be a direct process based on a direct $\chi^{(3)}$,

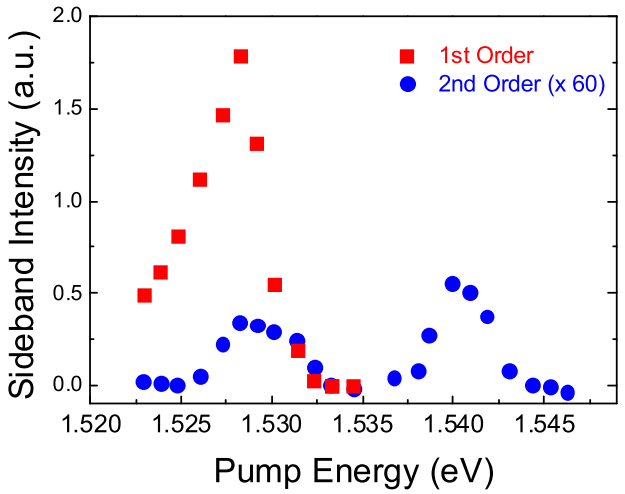

FIG. 3. Integrated spectra of each sideband as a function of NIR pump energy. The QCL was driven at 192 A/cm^2 with a duty cycle of 25% at 50 kHz. The second order intensity is multiplied by a factor of 60.

rather than an effective $\chi^{(3)}{}_{eff}$ process which would result from a cascaded second order nonlinear susceptibility $\chi^{(2)} \times \chi^{(2)}$.[20] The latter corresponds to the generation of a 1st order sideband, which in turn can generate another sideband through another THz photon (2nd order). For the case shown in Figure 1, when the pump is placed at the energy of the 1st order sideband, no signature of its own 1st order sideband is observed as the pump is not in resonance with the gap, ruling out the possibility of a cascaded second order effect. Instead, a direct third order process is observed as the 2nd order sideband occurs even when the 1st order sideband is below the interband transition and thus not in resonance with the bandgap.

Photoluminescence (PL) measurements (Figure 4(b)) were performed and compared with the simulated electron-heavy hole overlap (Figure 4(c)) and the sideband intensity (Figure 4(a)) to identify the origin of the resonances.[9] As the PL emission stems from transitions having the lowest energy, i.e., involving heavy holes states, it is compared to the sideband intensity for a TE polarization of the NIR pump (Figure 4(a)). The bandstructure of the device is shown in Figure 4(d). As in Ref. 21, the energy of the PL is red-shifted because of Joule heating of the QCL (around 2 W is applied to the QCL for these experiments) and this was taken into account by a 5 meV redshift of the calculated overlaps to coincide with the lowest simulated interband transition with the main peak of the PL (at 1.525 eV).[21] The first resonance in the sideband intensity for a TE pump excitation can be identified as being due to the transition in the largest well between the first confined heavy hole state ($|H1\rangle$ in Figure 4(b)) and the injector state of the QCL labelled $|E1\rangle/|E2\rangle$. The second resonance appears to fit with the transition $|H3\rangle|E4\rangle$. For both orders the strong absorption of the material above 1.521 eV plays an important role and prevents the observation of sidebands at higher energies.

The third order sideband shown in the inset of Figure 1 was observed at an energy of $E_{3rd} = E_{NIR} - 3E_{QCL} = 1.515$ eV with the NIR pump at an energy of 1.55 eV corresponding to resonances with higher subbands (Figure 4(c)). The sideband

Downloaded 04 Jun 2013 to 129.175.97.14. This article is copyrighted as indicated in the abstract. Reuse of AIP content is subject to the terms at: http://apl.aip.org/about/rights_and_permissions

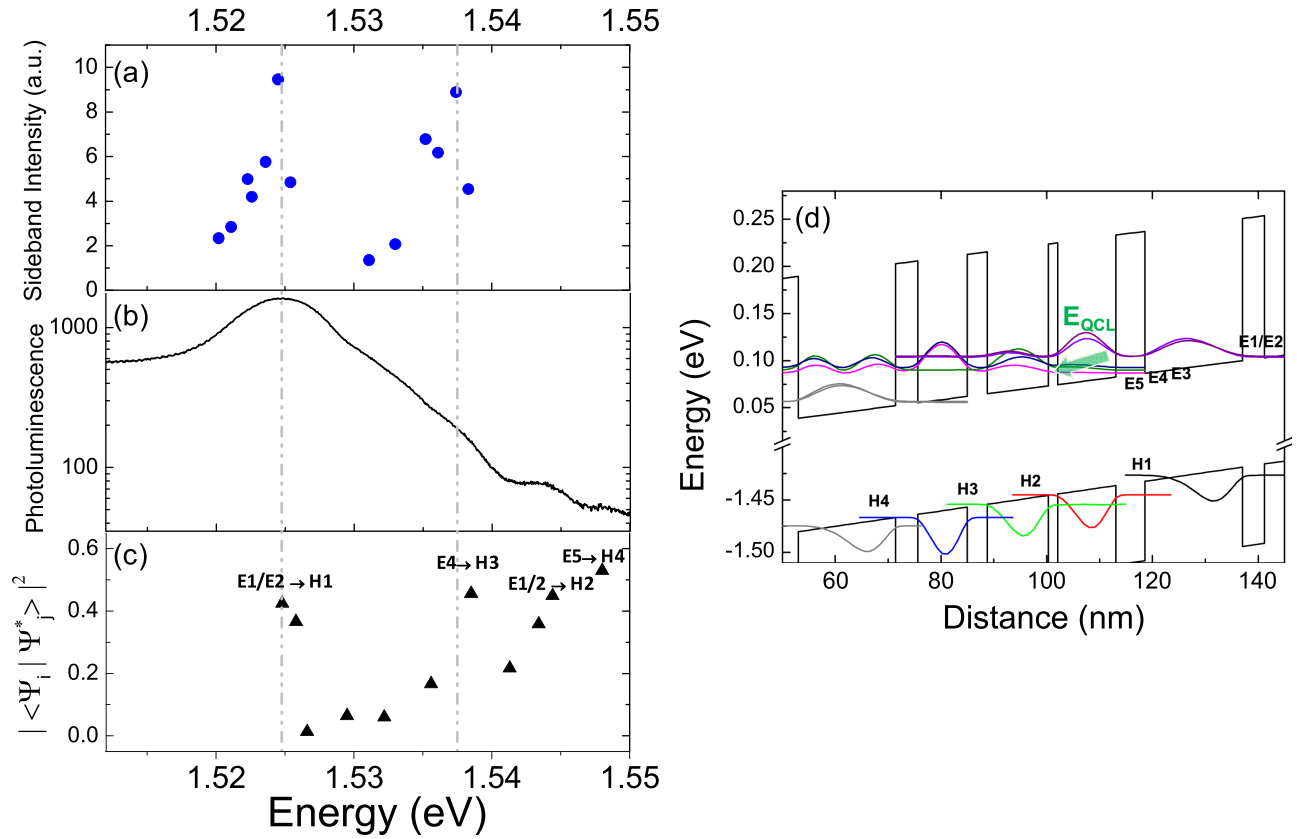

FIG. 4. (a) Second order sideband intensity as a function of the pump energy. The polarization of the NIR pump is TE implying predominant excitation of heavy holes. (b) Photoluminescence spectrum of the QCL biased above laser threshold. (c) Squared overlaps of the relevant interband transitions ($j \rightarrow k$) involving the kth heavy holes and jth electron states represented in the bandstructure of the QCL, as shown in panel (d). The QCL was driven at 173 A/cm^2 with a duty cycle of 25% at 50 kHz.

is observed close to the band edge, where the 1st and 2nd orders also appear with maximum intensity efficiency. This would correspond to a $\chi^{(4)}$ process although noise in the measurements prevents a quantitative analysis of the 3rd order harmonic intensity dependence on current density to confirm this. Indeed, the power of the 3rd harmonic is low (less than 0.1 pW).

In conclusion, we have demonstrated high-order sideband generation of an optical excitation in a THz QCL. This has been achieved by using the strong confinement of a THz field in double metal waveguides, resulting in large intracavity fields that permit the generation of sidebands from the 1st to 3rd order. Even higher order sidebands could be observed through a higher power QCL and through different excitation geometries (e.g., a split cavity scheme or reflective geometry) to avoid the absorption of the pump and generated beams.

We acknowledge financial support from the CNANO contract "TeraConversion," and from the French National Research Agency (ANR-09-NANO-017 "Hi-Teq"). The LPA-ENS is a "Unité Mixte de Recherche Associée au CNRS UMR8551 et aux Universités Paris 6 et 7." The device fabrication has been performed at the nano-center CTU-IEF-Minerve, which was partially funded by the Conseil Général de l'Essonne. We are grateful for support from the EPSRC (UK), the ERC programmes NOTES and TOSCA, and to the Royal Society and Wolfson Foundation. We are grateful to Iman Kundu for his help in characterising laser structures. We thank Nathalie Isac for help with the wafer-bonding process.

[1]J. Faist, F. Capasso, D. L. Sivco, C. Sirtori, A. L. Hutchinson, and A. Y. Cho, "Quantum cascade laser," Science **264**, 553–556 (1994).
[2]R. Köhler, A. Tredicucci, F. Beltram, H. E. Beer, E. H. Linfield, A. G. Davies, R. C. Iotti, and F. Rossi, Nature **417**, 156 (2002).
[3]E. Rosencher and Ph. Bois, Phys. Rev. B **44**, 11315 (1991).
[4]C. Sirtori, F. Capasso, J. Faist, L. N. Pfeiffer, and K. W. West, Appl. Phys. Lett. **65**, 445–447 (1994).
[5]N. Owschimikow, C. Gmachl, A. Belyanin, V. Kocharovsky, D. L. Sivco, R. Colombelli, F. Capasso, and A. Y. Cho, Phys. Rev. Lett. **90**, 043902 (2003).
[6]M. A. Belkin, F. Capasso, A. Belyanin, D. L. Sivco, A. Y. Cho, D. C. Oakley, C. J. Vineis, and G. W. Turner, Nat. Photonics **1**, 288 (2007).
[7]K. Vijayraghavan, R. W. Adams, A. Vizbaras, M. Jang, C. Grasse, G. Boehm, M. C. Amann, and M. A. Belkin, Appl. Phys. Lett. **100**, 251104 (2012).
[8]Q. Y. Lu, N. Bandyopadhyay, S. Slivken, Y. Bai, and M. Razeghi, Appl. Phys. Lett. **101**, 251121 (2012).
[9]J. Madéo, P. Cavalié, J. R. Freeman, N. Jukam, J. Maysonnave, K. Maussang, H. E. Beere, D. A. Ritchie, C. Sirtori, J. Tignon, and S. S. Dhillon, Nat. Photonics **6**, 519 (2012).
[10]J. Kono, M. Y. Su, T. Inoshita, M. S. Sherwin, S. J. Allen, Jr., and H. Sakaki, Phys. Rev. Lett. **79**(6), 1758–1761 (1997).
[11]S. G. Carter, V. Ciulin, M. S. Sherwin, M. Hanson, A. Huntington, L. A. Coldren, and A. C. Gossard, Appl. Phys. Lett. **84**(6), 840 (2004).
[12]B. Zaks, R. B. Liu, and M. S. Sherwin, Nature **483**(7391), 580 (2012).
[13]S. S. Dhillon, C. Sirtori, J. Alton, S. Barbieri, A. De Rossi, H. E. Beere, and D. A. Ritchie, Nature Photon. **1**, 411–415 (2007).

Downloaded 04 Jun 2013 to 129.175.97.14. This article is copyrighted as indicated in the abstract. Reuse of AIP content is subject to the terms at: http://apl.aip.org/about/rights_and_permissions

[14]C. Zervos, M. D. Frogley, C. C. Phillips, D. O. Kundys, L. R. Wilson, J. W. Cockburn, M. Hoptinkson, and S. Skolnick, Appl. Phys. Lett. **89**, 183507 (2006).
[15]S. G. Carter, V. Ciulin, M. Hanson, A. S. Huntington, C. S. Wang, A. C. Gossard, L. A. Coldren, and M. S. Sherwin, Phys. Rev. B **72**, 155309 (2005).
[16]S. Kumar and A. Lee, IEEE J. Sel. Top. Quantum Electron. **14**, 333 (2008).
[17]M. I. Amanti, G. Scalari, R. Terazzi, M. Fischer, M. Beck, J. Faist, A. Rudra, P. Gallo, and E. Kapon, New J. Phys. **11**, 125022 (2009).
[18]J.-Y. Bengloan, A. De Rossi, V. Ortiz, X. Marcadet, M. Calligaro, I. Maurin, and C. Sirtori, Appl. Phys. Lett. **84**, 2019 (2004).
[19]R. L. Sutherland, D. G. McLean, and S. Kirkpatrick, *Handbook of Nonlinear Optics* (CRC Press, 2003).
[20]J. B. Khurgin, A. Obeidat, S. J. Lee, and Y. J. Ding, J. Opt. Soc. Am. B **14**, 1977 (1997).
[21]M. S. Vitiello, G. Scamarcio, V. Spagnolo, B. S. Williams, S. Kumar, Q. Hu, and J. L. Reno, Appl. Phys. Lett. **86**, 111115 (2005).

Downloaded 04 Jun 2013 to 129.175.97.14. This article is copyrighted as indicated in the abstract. Reuse of AIP content is subject to the terms at: http://apl.aip.org/about/rights_and_permissions